Journal of Power Sources 195 (2010) 4853–4864

Contents lists available at ScienceDirect

Journal of Power Sources

journal homepage: www.elsevier.com/locate/jpowsour

Compatibility between AISI441 alloy interconnect and representative seal glasses in solid oxide fuel/electrolyzer cells

T. Jin, K. Lu*

Department of Materials Science and Engineering, Virginia Polytechnic Institute, State University, Blacksburg, VA 24061, USA

ARTICLE INFO

Article history:
Received 19 December 2009
Received in revised form 5 February 2010
Accepted 8 February 2010
Available online 12 February 2010

Keywords:
Solid oxide fuel/electrolyzer cell
Seal glass
Interconnect
Atmosphere
Thermal stability

ABSTRACT

AISI441 alloy, an advanced ferritic stainless steel, is considered as a promising metallic interconnect material for solid oxide fuel/electrolyzer cells. In this work, the compatibility between the AISI441 alloy and four representative seal glasses (YSO-4, G18, SABS-0, and SCAN2) has been studied. The AISI441/glass couples are thermally treated in both air and H_2/H_2O atmospheres at 800 °C for up to 500 h. Interfacial morphology shows that the YSO-4 glass and the SCAN2 glass have relatively high reaction tendency with the AISI441 alloy; the G18 glass devitrifies extensively during the thermal treatment; and the SABS-0 glass shows very little interaction or devitrification. In the H_2/H_2O atmosphere, the AISI441 alloy has less interaction with the sealing glasses compared with the air condition. Different phases from interfacial reaction and devitrification have been identified for each of the sealing glasses. Diffusion, devitrification, and reaction are the events occurring at the interface. Overall, the AISI441/SABS-0 glass couple shows the least interfacial reaction and devitrification and the best thermal stability.

1. Introduction

Solid oxide fuel/electrolyzer cells (SOFCs/SOECs) have been actively studied, either as a clean and efficient energy conversion device (for SOFCs) or as a H_2 producing device (for SOECs). These SOFCs/SOECs have the great potential of producing clean energy or clean synthetic fuel [1]. However, they are composed of very different components. The electrolyte materials are mostly stabilized cubic zirconia with low coefficient of thermal expansion (CTE). The electrode materials are either low CTE ceramics or metal–ceramic composites [2]. The interconnect materials are metal alloys with a much higher CTE. Different cell components need to be hermetically sealed at all times in order to prevent gas mixing, leakage, or internal combustion. This requirement places extreme demands on a seal glass to perform in severe environments involving high temperatures, thermal stress, and chemically aggressive conditions [3–6]. Undesirable interaction at the metal/glass interface can lead to cracking of the seal glass and mixing of fuel and oxygen containing gases [7–10]. The interconnect/glass sealant interfacial behavior is also affected by different atmospheres. These issues are often exacerbated by long-term operation (>40,000 h), high temperatures (750–900 °C), and corrosive atmospheres (wet reducing), which frequently drive materials into regimes where conventional understanding of material behaviors and transport processes is not sufficient.

Intensive research effort has been undertaken to address SOFC/SOEC high temperature diffusion, reaction, and degradation issues [11]. For the metallic interconnect, most studies are focused on ferritic stainless steel [8–14], which has 11.0–12.5 × 10^{-6} K^{-1} CTE. Chromium is the necessary ingredient in the interconnect to reduce oxidation under SOFC/SOEC operating conditions [8]. Crofer 22 APU, a commercial Fe–Cr–Mn steel with 11.5 × 10^{-6} K^{-1} CTE, shows good chemical compatibility with glass sealants [13,14]. However, migration of Cr-containing species from the metallic interconnect to the seal glass causes serious chemical and microstructural stability problems and shortens the lifetime of SOFCs/SOECs [15]. A protective $(Mn,Cr)_3O_4$ spinel coating has been applied on the surface of the Crofer 22 APU alloy to decrease the diffusion of chromium [16]. However, the procedure requires dedicated coating efforts and increases cell complexity and cost. An additional issue is that the Crofer 22 APU alloy itself is expensive and not widely available, especially in the United States. AISI441, a similar alloy with higher yield strength and lower cost [17], is being considered as an alternative interconnect material. However, there are many unknowns for the AISI441 alloy. The immediate question is the chemical compatibility between the AISI441 alloy and a sealant glass.

Seals must be chemically and structurally stable at SOFC/SOEC high temperature reactive environments (moist reducing and/or oxidizing conditions), and demonstrate chemical compatibility

* Corresponding author. Tel.: +1 540 231 3225; fax: +1 540 231 8919.
E-mail address: klu@vt.edu (K. Lu).

0378-7753/$ – see front matter © 2010 Elsevier B.V. All rights reserved.
doi:10.1016/j.jpowsour.2010.02.015

with interconnect materials [18–24]. Also, seals should have good bonding with the cell components that they seal. In addition, a seal glass must have high devitrification resistance. Volatile constituents (e.g., alkaline oxides) should be avoided. If any volatile species is present, it should not have a deleterious effect on cell performance. From all the seal glass candidates reported in the literature, four glass compositions can be identified to represent the full range of glass sealants.

The first is the YSO-4 glass reported by Chou et al. [25], which contains 34 mol% SiO_2, 7.5 mol% B_2O_3, 5 mol% CaO, 47.5 mol% SrO, and 6 mol% Y_2O_3. The CTE of the YSO-4 glass is $11.7 \times 10^{-6}\,K^{-1}$. The glass transition temperature T_g is relatively high, at ~713 °C. The incentive for developing this glass is to utilize the "refractory" ingredients to minimize interfacial reactions while maintaining long-term thermal stability. The approach is based on the premise that the larger the temperature difference between the sealing temperature, e.g., 950 °C, and the cell operating temperature, e.g., 750 °C, the less the interfacial reaction and the greater the thermal stability are during long-term operation. However, this glass devitrifies extensively after thermal treatment at 900 °C. When it comes in contact with a metallic interconnect at 900–1050 °C in air, microstructure analysis reveals the presence of $SrCrO_4$ near the metal/glass–ceramic interface [25].

The second glass is a BaO-rich aluminoborosilicate glass. Alkaline-earth oxides are used to increase the CTE of such seal glass systems. In this category, the most studied system is G18 glass reported by Yang et al. [9] and Meinhardt et al. [26]. This glass contains 35 mol% SiO_2, 10 mol% B_2O_3, 5.0 mol% Al_2O_3, 15 mol% CaO, and 35 mol% BaO. The CTE of this glass is $11.8 \times 10^{-6}\,K^{-1}$. The T_g of this glass is intermediate, ~630 °C. This glass also devitrifies extensively after thermal treatment at 750 °C [26]. The glass–ceramic system has a CTE of $10.8 \times 10^{-6}\,K^{-1}$. The idea of using this glass as a sealing material is to utilize a mixture of glass and ceramic phases to provide the sealing and bonding strength. However, the interactions with metal components are extensive and dependent on the composition of the metal oxide scale that forms during sealing [26]. Alumina-scale formers exhibit a more compact reaction zone with the glass than chromia-scale forming alloys. Of greater concern is the interfacial strength between the sealant and the metallic component, which is dependent on the extent of interaction between the two materials as a function of time and temperature under different atmospheres.

The third glass is the SABS-0 glass reported by us [27]. This glass contains SiO_2, La_2O_3, Al_2O_3, and SrO and is purposely designed to be BaO- and B_2O_3-free. This is also an intermediate temperature sealant. The glass desirably has 775 °C T_g and 815 °C glass softening temperature T_d. It is thermally stable after being kept at 850 °C for 200 h [27] and at 800 °C for 1000 h [28]. Ni addition into the SABS-0 glass can effectively lower T_g and T_d while not substantially affecting the CTE and thermal stability. Interfacial compatibility and thermochemical stability are studied for the SABS-0 and Crofer 22 APU interconnect system. The variables examined include thermal treatment temperature (700–850 °C) and time (0–100 h). Pore- and crack-free interface is obtained and maintained for all the thermal treatment conditions. There are simultaneous but minor diffusion of the Crofer 22 APU elements and the SABS-0 elements, chemical reaction at the Crofer 22 APU/SABS-0 interface, and devitrification of the SABS-0 glass itself. The diffusion distance is the highest for chromium at ~7 μm under the studied thermal treatment conditions [29].

The fourth glass is the SCAN2 glass reported by Smeacetto et al. [30], which contains 40 mol% SiO_2, 10 mol% B_2O_3, 9.0 mol% Al_2O_3, 18 mol% CaO, and 23 mol% Na_2O. The CTE is $11.2 \times 10^{-6}\,K^{-1}$. The T_g is ~545 °C. This is a low temperature seal glass for SOFCs/SOECs. This glass devitrifies extensively after thermal treatment at 800 °C. The joining process at 900 °C causes partial surface devitrification of the glass, resulting in a glass–ceramic seal. Thermal treatment in air (800 °C, 400 h) causes Cr diffusion from the Crofer 22 APU alloy to the seal.

Even though the above studies have individually attempted to explore the potentials of these four different sealing glasses, the experiments have been conducted under different conditions and using different interconnect materials. There is a lack of comparison about the stability and effectiveness of these glasses as sealing materials. This study is to evaluate the interfacial compatibility and phase changes of these four sealing glasses under the same thermal treatment conditions and with the same interconnect material, the AISI441 alloy. The experiments have been carried out in air and wet hydrogen atmospheres at 800 °C for up to 500 h. The elemental inter-diffusion, the interfacial reaction between the individual glass and the AISI441 alloy, and the devitrification of each glass are discussed.

2. Experimental procedure

2.1. Glass preparation

All the glasses were prepared with the conventional glass manufacturing process by mixing oxides and carbonates in a ball mill overnight and melting the mixture in a platinum crucible in a box furnace (Lindberg, Model No. 51314, Watertown, WI). All chemicals were from Alfa Aesar, Ward Hill, MA, except for $SrCO_3$, which was from Sigma–Aldrich, St. Louis, MO. For the YSO-4 glass, $SrCO_3$ (99.9%), Y_2O_3 (99.99%), $CaCO_3$ (99.95–100.05%), B_2O_3 (99.99%), and SiO_2 (99.8%) at the designed composition were mixed and melted at 1500 °C for 2 h [25]. For the G18 glass, $CaCO_3$ (99.95–100.05%), $BaCO_3$ (99.8%), B_2O_3 (99.99%), and SiO_2 (99.8%) at the designed composition were mixed and melted at 1300 °C for 3 h [26]. For the SABS-0 glass, $SrCO_3$, La_2O_3 (99.98%), Al_2O_3 (99.95%), and SiO_2 (99.8%) at the designed composition were mixed and melted at 1400 °C for 4 h [27]. For the SCAN2 glass, Al_2O_3 (99.95%), $NaCO_3$ (99.95–100.05%), $CaCO_3$ (99.95–100.05%), B_2O_3 (99.99%), and SiO_2 (99.8%) at the designed composition were mixed and melted at 1500 °C for 1 h [30]. The molten glasses were quenched into a graphite mold. The glasses were cut into thin pieces.

2.2. Glass-interconnect bonding

AISI441 ferritic stainless steel (ATI Allegheny Ludlum Corporation, Brackenridge, PA) with a chemical composition (wt%) of Cr 17.6%, Mn 0.33%, Ti 0.18%, Si 0.47%, Al 0.045%, C 0.01%, S 0.001%, P 0.024%, Ni 0.20%, Nb 0.46%, and Fe 80.68% was prepared as rectangular substrates. Bare AISI441 samples were polished to optical finish to remove the oxidized layer, if any, and to obtain scratch free flat surface. The polished samples were cleaned by ultrasound in water first and then in acetone. The cleaned metal substrates were dried and wiped with acetone to get a clean surface. The same sized thin glass pieces (19 mm × 19 mm × 2 mm) for each of the four glasses were put on the polished metal surfaces. The AISI441/glass couples were heated in a box furnace (Lindberg, Model No. 51314, Watertown, WI) in air without any load. AISI441/YSO-4 was bonded at 1075 °C for 1 h, AISI441/G18 and AISI441/SABS-0 were bonded at 925 °C for 30 min, and AISI441/SCAN2 was bonded at 1000 °C for 30 min. The heating rate was 5 °C min^{-1} for the AISI441/G18 and AISI441/SABS-0 samples, and 10 °C min^{-1} for the AISI441/YSO-4 and AISI441/SCAN2 samples. The cooling rate was 3 °C min^{-1} for all the bonding experiments.

2.3. Glass-interconnect interfacial study

The AISI441/YSO-4, AISI441/G18, AISI441/SABS-0, and AISI441/SCAN2 samples were thermally treated at 800 °C for different dwell

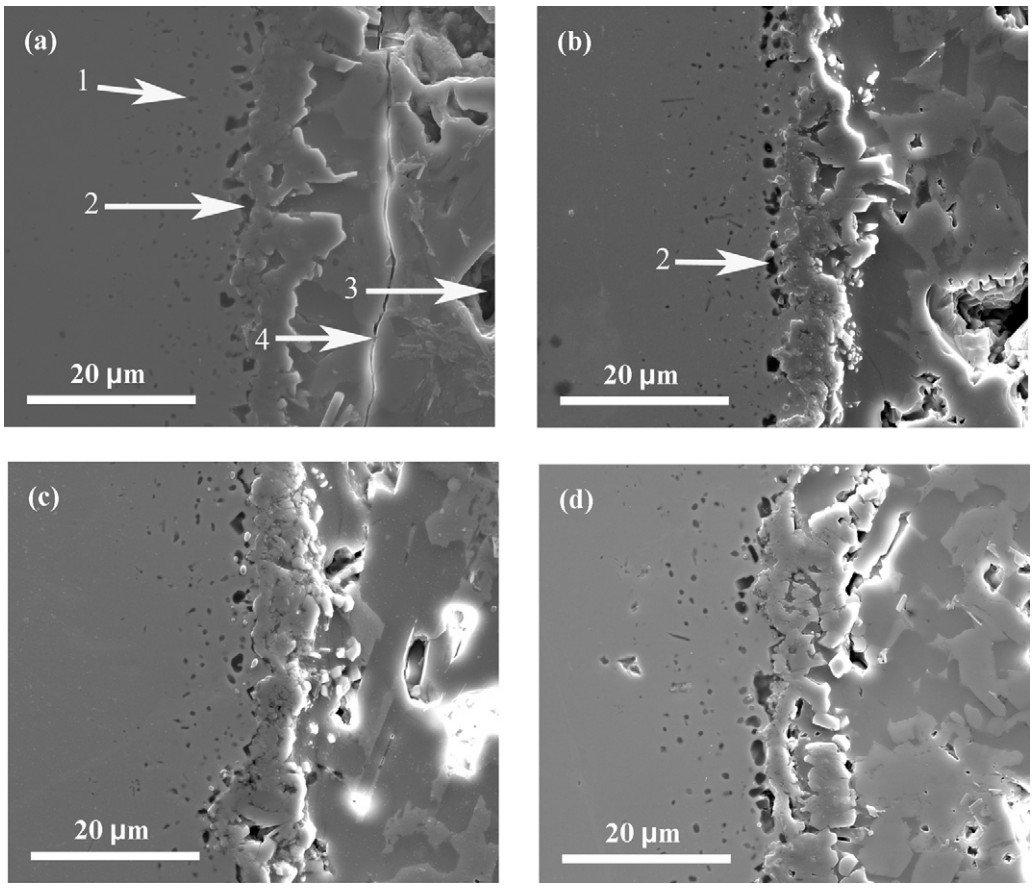

Fig. 1. Cross-section SEM images of the AISI441/YSO-4 glass couple interface before and after thermal treatment at 800 °C in air: (a) as-bonded, (b) 100 h, (c) 200 h, and (d) 500 h. In each image, the left side is the AISI441 alloy and the right side is the YSO-4 glass.

times up to 500 h in air and wet hydrogen (H_2/H_2O) atmospheres. The heating and cooling rates for all the thermal treatment were 3 °C min^{-1}. The wet hydrogen atmosphere was created by flowing hydrogen through a water container maintained at 83 °C. This temperature created ~50% water vapor in the gas mixture. The H_2/H_2O gas flow tube was maintained at 83 °C by hot tapes in order to avoid water condensation.

2.4. Microstructure and phase characterization

To study the AISI441/YSO-4, AISI441/G18, AISI441/SABS-0, and AISI441/SCAN2 sample interfacial microstructure evolution at different thermal treatment times and atmospheres, the thermally treated AISI441/glass samples were finely polished to optical finish. Field emission scanning electron microscopy (SEM, FEI Quanta 600 FEG, Hillsboro, OR) was used to examine the microstructures of the glasses and the interfacial microstructures of the AISI441/YSO-4, AISI441/G18, AISI441/SABS-0, and AISI441/SCAN2 samples. The accelerating voltage for the SEM experiments was 20 kV and secondary electron images were collected.

To investigate the devitrified phases at the interfaces of the AISI441/YSO-4, AISI441/G18, AISI441/SABS-0, and AISI441/SCAN2 samples, high-resolution X-ray diffraction (XRD) studies were carried out in an X'Pert PRO diffractometer (PANalytical B.V., EA Almelo, The Netherlands). The glass coated AISI441 surfaces were polished to 15–20 μm glass layer thickness. Such YSO-4, G18, SABS-0, and SCAN2 glass layer thicknesses were deemed suitable since X-ray detects 95% of the phase information from 25 μm penetration depth [31]. The scan time per step was 3000 s with CuK_α radiation (λ = 1.5406 Å).

3. Results and discussion

3.1. Interfacial microstructures

YSO-4 is a high temperature sealing glass that has to be bonded with the AISI441 interconnect at >1000 °C. Y_2O_3 makes the YSO-4 glass highly vulnerable to devitrification [25]. The SEM cross-section images of the AISI441/YSO-4 glass couple before and after the thermal treatment at 800 °C in air for 100 h, 200 h, and 500 h are given in Fig. 1. Even at the as-bonded condition (Fig. 1(a)), small, dark spots (marked as 1) can be seen on the metal side far away from the interface, which are believed to be caused by the oxidation of Ti in the AISI441 alloy [32]. Closer to the interface, larger size pores (marked as 2) are also observed on the AISI441 side. They are believed to come from the vaporization of Cr in the AISI441 alloy [17]. On the glass side, the YSO-4 glass partially devitrifies and large pores (marked as 3) form after bonding. Phase separation is also evident on the glass side. The long, vertical crack (marked as 4) in Fig. 1(a) is believed to be created during polishing, not part of the interfacial interaction. An interfacial layer of ~10 μm thickness forms between the metal and the glass with rough interfacial boundaries. After 100 h of thermal treatment (Fig. 1(b)), the larger pores (marked as 2) on the metal side persist and more devitrification and phase separation occur in the glass. However, the overall microstructure changes during the thermal treatments are not significant for the thermal treatment time up to 500 h (Fig. 1(d)). This is likely because the high bonding temperature of 1075 °C for the AISI441/YSO-4 couple has already caused the most extensive interfacial interaction. The thermal treatment at 800 °C plays a less significant role for the interfacial changes. This is also consistent

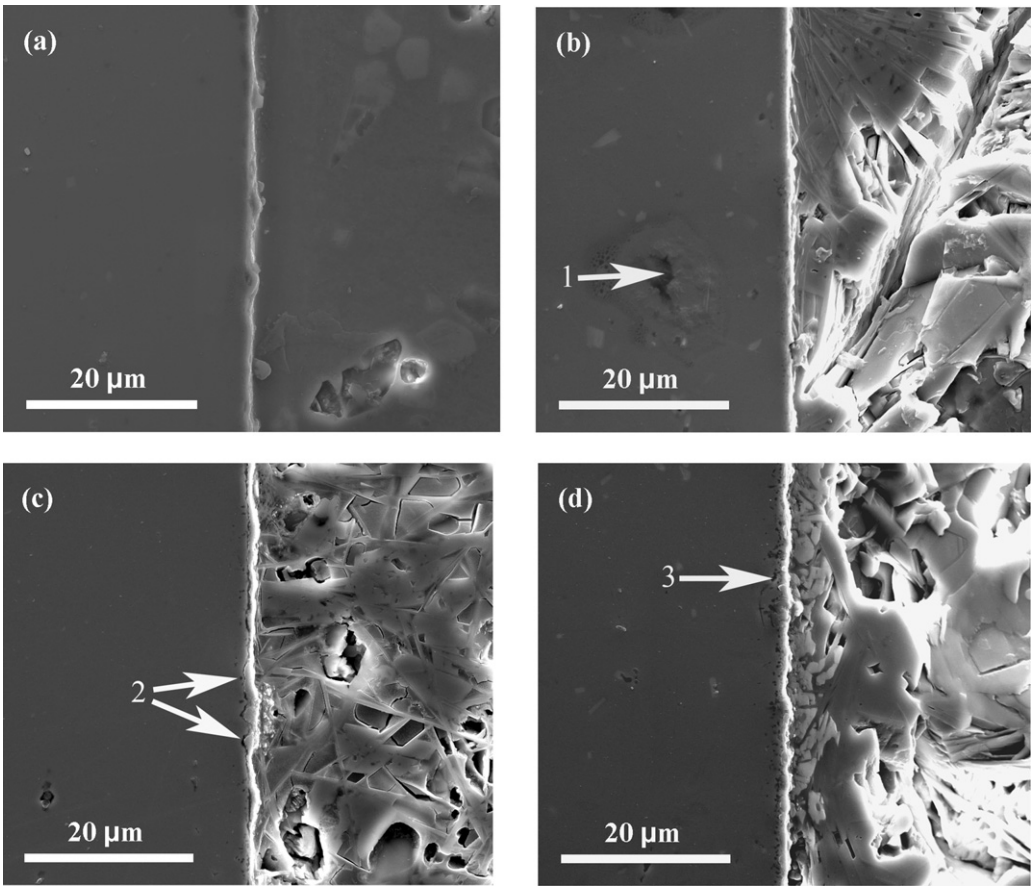

Fig. 2. Cross-section SEM images of the AISI441/G18 glass couple interface before and after thermal treatment at 800 °C in air: (a) as-bonded, (b) 100 h, (c) 200 h, and (d) 500 h. In each image, the left side is the AISI441 alloy and the right side is the G18 glass.

with the understanding that YSO-4 is a high temperature sealing glass. The microstructure changes and interfacial interaction are less significant at 800 °C.

The cross-section SEM images of the AISI441/G18 glass couple before and after the thermal treatment at 800 °C in air for 100 h, 200 h, and 500 h are given in Fig. 2. At the as-bonded state (Fig. 2(a)), the G18 glass forms an intimate interface with the AISI441 alloy with a sharp and even boundary. No pores, cracks, or interaction layer can be seen. This means both the AISI441 alloy and the G18 glass are stable during the bonding process. After 100 h of thermal treatment, the G18 glass shows extensive devitrification (Fig. 2(b)). Layered crystalline phases form on the glass side. Pores and cracks can be easily seen in the crystalline phase. Some large pores (marked as 1) also appear on the AISI441 alloy side far from the interface, but these pores seem to initiate from local AISI441 pitting (likely minor alloy composition oxidation and pull-out during polishing), different from the pores seen in the AISI441/YSO-4 samples. For the 200 h thermally treated sample (Fig. 2(c)), small pores/cracks (marked as 2) appear on the metal side near the interface, indicating that the reaction layer has poor compatibility with the AISI441 alloy. The glass side shows needle-like crystalline phases and extensive pore formation. This means the G18 glass has poor thermal stability and sealing ability at SOFC/SOEC operating conditions. After 500 h of thermal treatment (Fig. 2(d)), the small pores (marked as 3) in the AISI441 alloy continue to be present. The interfacial layer increases in thickness and even dissolves into the G18 glass. The high contrast of the dissolving phase indicates the presence of some high atomic number species. On the glass side the crystalline phase continues to evolve.

The SEM cross-section images of the AISI441/SABS-0 glass couple before and after the thermal treatment at 800 °C in air for 100 h, 200 h, and 500 h are given in Fig. 3. After being bonded in air at 925 °C (Fig. 3(a)), the AISI441 alloy and the SABS-0 glass form an intimate interface with a sharp and straight boundary. There are some minor pitting spots (marked as 1) on the AISI441 side but no pores from Cr vaporization or interfacial reaction are observed. A layer of 10–20 μm thickness with needle-shaped microstructure is seen on the SABS-0 glass side. This indicates that the SABS-0 glass near the AISI441 alloy is less stable and devitrifies during the bonding process. The interfaces after the thermal treatment for 100 h (Fig. 3(b)) and 200 h (Fig. 3(c)) show almost no difference from the as-bonded condition. The thickness of the crystalline phase on the glass side is still around 20 μm. This means the AISI441/SABS-0 interface is very stable. After 500 h (Fig. 3(d)) of thermal treatment, some round-shaped features (marked as 2) appear on the SABS-0 glass side near the interface. Away from the interface, the features on the glass side gradually transform into elongated shapes (marked as 3). The crystalline phase regions still stay at ~20 μm thick but the feature sizes are larger than the needle-shaped crystalline phase for the as-bonded and the shorter thermal treatment conditions (Fig. 3(a)–(c)). This means long-term thermal treatment does cause slow devitrification of the SABS-0 glass. The devitrified phase morphology is related to the interface. The needle-shaped crystals have been observed on the polished SABS-0 glass surface after thermal treatment in both air and H_2/H_2O atmospheres [28]. The round-shaped crystals are only observed when the SABS-0 glass is in contact with the AISI441 alloy. For all the conditions studied, no pores or cracks are observed on the AISI441 alloy side near or at the interface. There

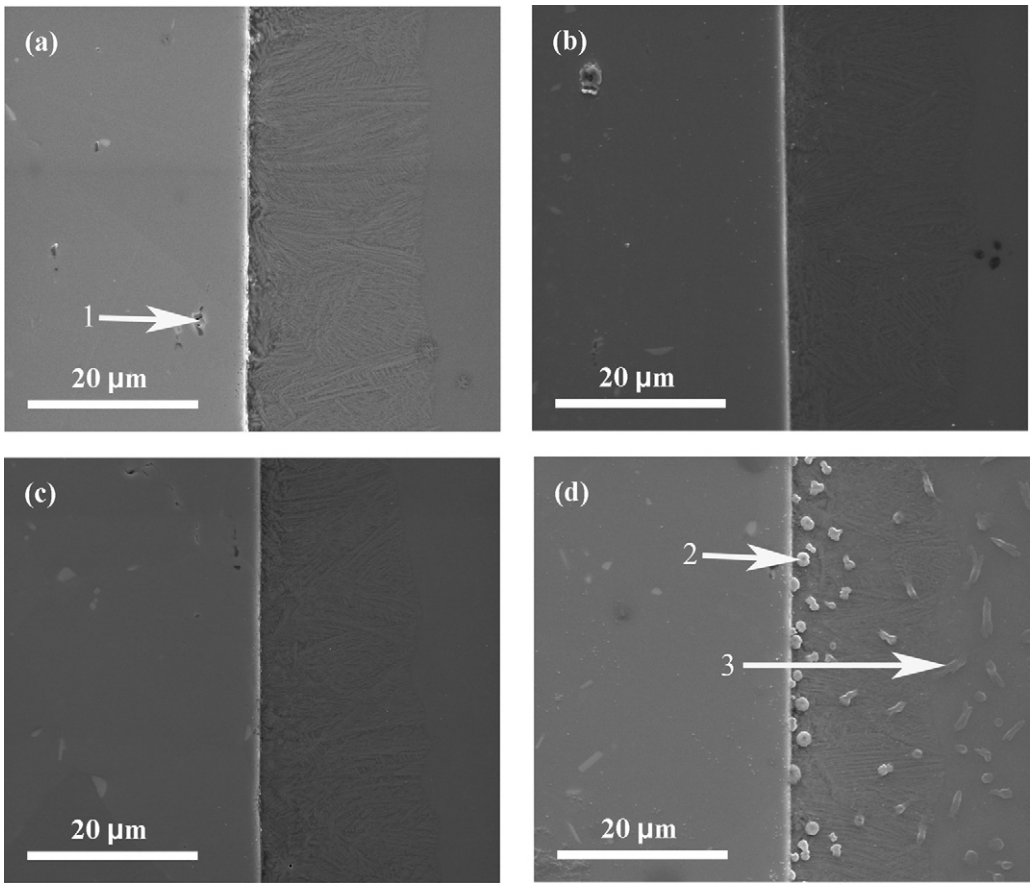

Fig. 3. Cross-section SEM images of the AISI441/SABS-0 glass couple interface before and after thermal treatment at 800 °C in air: (a) as-bonded, (b) 100 h, (c) 200 h, and (d) 500 h. In each image, the left side is the AISI441 alloy and the right side is the SABS-0 glass.

is no obvious reaction between the AISI441 alloy and the SABS-0 glass.

The SEM cross-section images of the AISI441/SCAN2 glass couple before and after the thermal treatment at 800 °C in air for 100 h, 200 h, and 500 h are given in Fig. 4. An interfacial layer can be seen at the interface for all the thermal treatment conditions. The reaction layer is wide with random variation and porous morphology. New phases are formed at the interface. At the as-bonded condition (Fig. 4(a)), small pores (marked as 1) form on the metal side and along the interfacial layer but the cause is difficult to identify from the microstructures. On the glass side, extensive devitrification occurs. After 100 h of thermal treatment (Fig. 4(b)), large pores (marked as 2) appear on the SCAN2 glass side. As the thermal treatment time increases to 200 h (Fig. 4(c)), more pores (marked as 3) appear at the interface on the metal side and phase separation occurs in the SCAN2 glass. With the thermal treatment time increase to 500 h (Fig. 4(d)), the interfacial layer grows even thicker. The SCAN2 glass shows extensive phase separation, devitrification, and pore formation. This means that the SCAN2 glass has poor thermal stability and compatibility with the AISI441 alloy.

As shown in Fig. 1(a) for the AISI441/YSO-4 couple, extensive devitrification and pore formation occur on the YSO-4 glass side after being bonded with the AISI441 alloy at 1075 °C for 1 h; and closed pores on the metal side are also apparent. The SEM cross-section images of the AISI441/YSO-4 glass couple after the thermal treatment at 800 °C in the H_2/H_2O atmosphere for 100 h, 200 h, and 500 h are given in Fig. 5. The thermal treatment in the H_2/H_2O atmosphere causes more extensive devitrification and crack formation than the air condition. Tiny, dark spots (marked as 1) are observed on the AISI441 side and believed to be from Ti oxidation. Slightly larger pores (marked as 2) are observed on the AISI441 side at the interface. These larger pores are likely from Cr vaporization. The interfacial layer is also much wider and more poorly defined with large cracks (marked with 3) inside the interfacial layer. Devitrification and phase separation are severe on the YSO-4 glass side. This means that the YSO-4 glass cannot form good bonding with the AISI441 alloy under the wet reducing atmosphere. The widespread pores/cracks indicate that there will be problems during sealing and cell operation.

The SEM cross-section images of the AISI441/G18 glass couple after the thermal treatment at 800 °C for 100 h, 200 h, and 500 h in the H_2/H_2O atmosphere are given in Fig. 6. The AISI441 alloy side shows excellent microstructural stability at all the H_2/H_2O thermal treatment conditions. No pores are seen on the AISI441 alloy side. Clear and even interfacial boundaries are also maintained. These observations indicate that the wet hydrogen reducing atmosphere can reduce the pitting of the AISI441 alloy and its interaction with the G18 glass. However, the G18 glass side has similar microstructures as those of the samples thermally treated in air (Fig. 2(b)–(d)). Devitrified, layered crystalline phases dominate with a large number of cracks. After 100 h (Fig. 6(a)), the devitrification of the G18 glass is complete. Small cracks (marked as 1) can be observed along the layered crystalline phases. When the thermal treatment time increases to 200 h (Fig. 6(b)), thin cracks evolve into micron-sized long pores (marked as 2). This phenomenon (marked as 3) persists and is still prevalent for the 500 h thermally treated sample (Fig. 6(c)).

The SEM cross-section images of the AISI441/SABS-0 glass couple after the thermal treatment at 800 °C for 100 h, 200 h, and 500 h in the H_2/H_2O atmosphere are given in Fig. 7. Similar to the samples

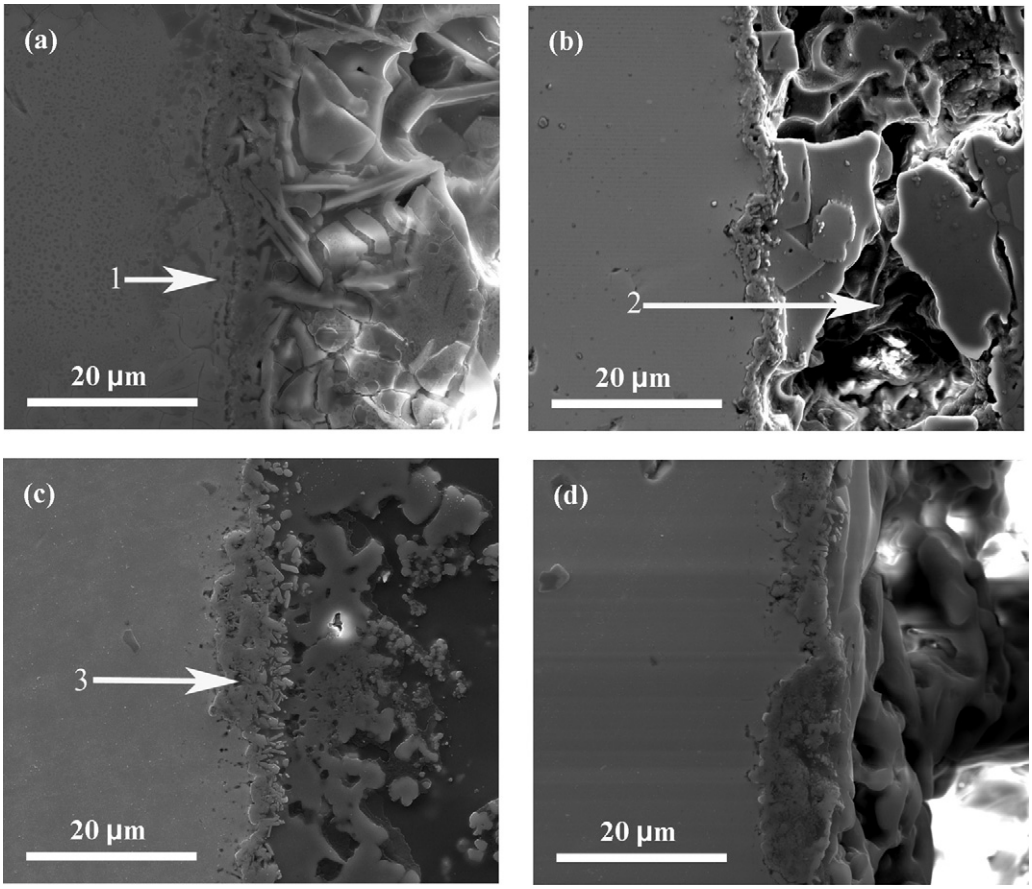

Fig. 4. Cross-section SEM images of the AISI441/SCAN2 glass couple interface before and after thermal treatment at 800 °C in air: (a) as-bonded, (b) 100 h, (c) 200 h, and (d) 500 h. In each image, the left side is the AISI441 alloy and the right side is the SCAN2 glass.

thermally treated in air (Fig. 3), a clear and even interface between the AISI441 alloy and the SABS-0 glass is maintained with no visible reaction. After the thermal treatment, the interface shows no obvious change compared to that of the as-bonded sample (Fig. 7 vs. Fig. 3(a)). Both the metal side and the glass side of the interface are free of any pores or cracks. The partially devitrified layer on the SABS-0 glass side also stays unchanged for 100 h (Fig. 7(a)), 200 h (Fig. 7(b)), and 500 h (Fig. 7(c)), at <20 μm thickness. Some very small and needle-shaped phases (marked as 1) form on the glass side of the interface after 500 h of thermal treatment (Fig. 7(d)). But the extent is much less than that of the 500 h thermally treated sample in air (Fig. 3(d)). This means that the wet reducing atmosphere (H_2/H_2O) can decrease the interaction between the AISI441 alloy and the SABS-0 glass at the interface, which is similar to the results seen for the AISI441/G18 sample. More importantly, the SABS-0 glass shows to be the most stable sealing glass when in contact with the AISI441 alloy.

Fig. 8 shows the SEM cross-section images of the AISI441/SCAN2 glass couple interface after the thermal treatment at 800 °C in the H_2/H_2O atmosphere. An extensive interaction layer forms after just being bonded at 1000 °C (Fig. 4(a)). Similar to the thermal treatment results in air, large pores (marked as 1) are also seen on the glass side for the H_2/H_2O thermal treatment conditions (Fig. 8). At the 100 h thermal treatment condition (Fig. 8(a)), the number of small pores on the AISI441 alloy side substantially diminishes. An interfacial layer forms between the AISI441 alloy and the SCAN2 glass. Also, some bright secondary phase forms in the SCAN2 glass close to the interface after 200 h of thermal treatment (Fig. 8(b) and (c)). Phase separation in the SCAN2 glass itself is extensive. After the thermal treatment in the H_2/H_2O atmosphere for 200 h (Fig. 8(b)) and 500 h (Fig. 8(c)), there are much fewer small pores on the metal side of the interface than those of the air treatment conditions. This indicates that the H_2/H_2O atmosphere can inhibit Ti oxidation and Cr vaporization. The interfacial layer is 5–15 μm. But some reaction products at the interface seem to be dissolving into the glass. The contrast difference in Fig. 8(b) and (c) shows that some high atomic number species participate in the reaction and diffusion into the glass. The SCAN2 glass phase separation is extensive. The phase separation and reaction of the SCAN2 glass, albeit less severe than the air treatment condition, indicate that the SCAN2 glass is a poor sealant.

3.2. Interfacial phase analysis

For the XRD analysis of the AISI441/glass interfacial crystalline phases, the XRD pattern for the AISI441 alloy is obtained first and used as a reference. For each as-bonded or thermally treated AISI441/glass sample, the presence of the characteristic XRD peak of iron at 44.67° confirms that the XRD patterns include all the crystalline phases across the interface. For brevity, only the results from the 500 h thermal treatment conditions are presented.

Fig. 9 shows the XRD patterns of the AISI441/YSO-4 samples at as-bonded, 500 h of thermal treatment in air, and 500 h of thermal treatment in the H_2/H_2O atmosphere conditions. The YSO-4 glass quickly devitrifies during the bonding process. Very significant crystalline peaks can be seen for the as-bonded sample. The thermal treatment at 800 °C in either air or the H_2/H_2O atmosphere does not significantly change the devitrified phases at the AISI441/YSO-4 interface; the main crystalline peaks stay the same. The main devitrified phases are $SrSiO_3$, Ca_3SiO_5, and Ca_2SiO_4, and

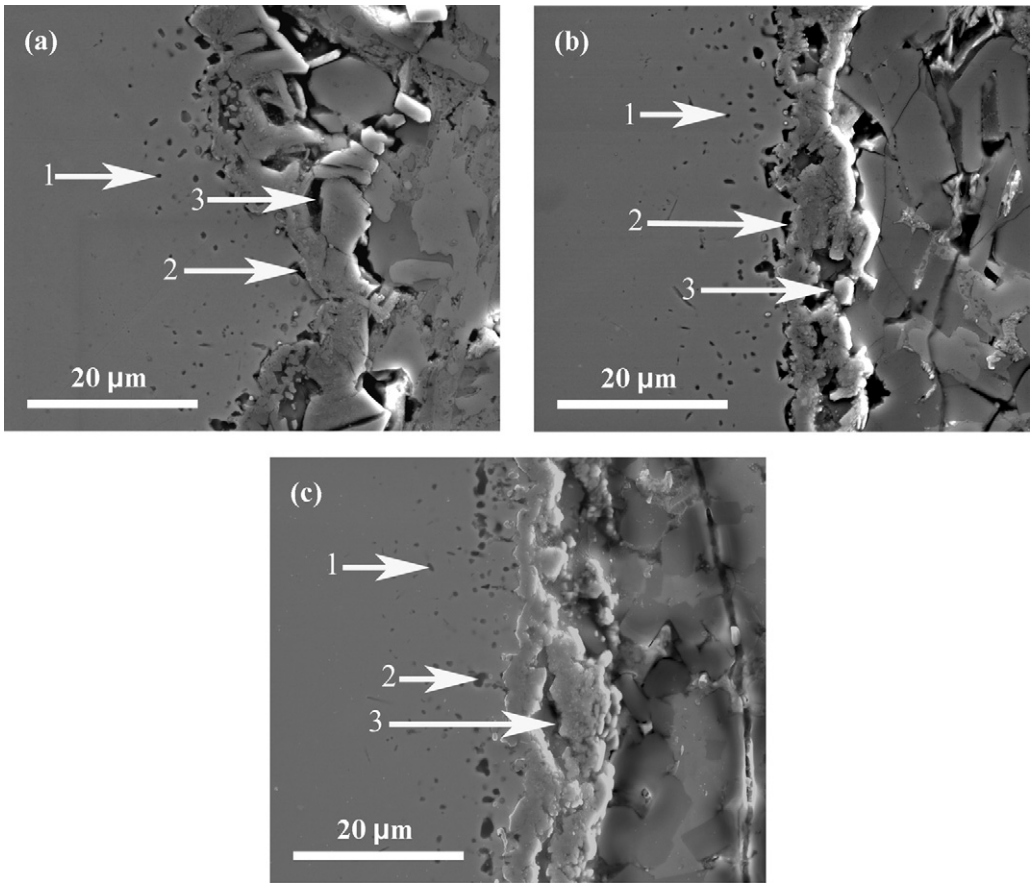

Fig. 5. Cross-section SEM images of the AISI441/YSO-4 glass couple interface after thermal treatment at 800 °C in H_2/H_2O atmosphere: (a) 100 h, (b) 200 h, and (c) 500 h. In each image, the left side is the AISI441 alloy and the right side is the YSO-4 glass.

the minor devitrified phases are $SrCrO_4$, Sr_2CrO_4, and Y_2SiO_5, along with some unknown phases.

$SrSiO_3$ has the highest peak intensity, peak number, and thus the highest crystalline content. This can be understood as follows. Silicate structural units are the glass formers for the YSO-4 glass. However, the YSO-4 glass has a high content of SrO and reasonable amounts of CaO and Y_2O_3. These species are very likely to react with the silicate groups and lead to new phase formation. $SrSiO_3$ forms from the thermodynamically unstable Sr^{2+} ions and silicate structural units in the glass network. Ca^{2+} ions from the YSO-4 glass also react with the silicate structural units and form Ca_3SiO_3 and Ca_2SiO_4. In air, CrO_3 vapor is the diffusing species for Cr [33]. The Cr species from the AISI441 alloy reacts with the YSO-4 glass and leads to the formation of a small amount of $SrCrO_4$. When the sample is thermally treated in air, accelerated Cr diffusion and interaction with the YSO-4 glass lead to the increase of the $SrCrO_4$ peak intensity. In contrast, the $SrCrO_4$ peak disappears after the thermal treatment in the H_2/H_2O atmosphere because the reducing atmosphere suppresses the vaporization and thus diffusion of Cr-containing species. The reaction product is Sr_2CrO_4 where Cr^{6+} ions are likely reduced to Cr^{4+} in the H_2/H_2O atmosphere. The peaks of the Sr_2CrO_4 phase overlap with those of the $SrSiO_3$ phase in the XRD pattern. More characterization is needed if the stability of Sr_2CrO_4 needs to be understood. For both the air treatment and the H_2/H_2O treatment conditions, the Y^{3+} ions from the YSO-4 glass also react with the silicate structural units and form Y_2SiO_5. From the devitrified species, it can be concluded that devitrification of the YSO-4 glass is the dominant event at the AISI441/YSO-4 interface. Cr-containing species diffusion in the air condition exacerbates this process.

The XRD patterns of the AISI441/G18 samples are shown in Fig. 10. At the as-bonded state, the devitrified phases are $BaCrO_4$, $BaFeSi_4O_{10}$, Al_2SiO_4, and some minor unknown phases. The $BaCrO_4$ peaks are weak and a result of reaction between the BaO in the G18 glass and the CrO_3 diffusing species from the AISI441 alloy. Al_2SiO_4 forms because of the devitrification of the G18 glass itself. $BaFeSi_4O_{10}$ forms because Cr and Fe species diffuse from the AISI441 alloy into the glass and react with the Ba^{2+} containing species. After 500 h of thermal treatment in air, the amounts of $BaFeSi_4O_{10}$ and Al_2SiO_4 phases increase because the interfacial reaction and the glass devitrification persist under this condition. The intensities of the $BaCrO_4$ peaks increase more significantly, indicating the formation of $BaCrO_4$ continues under this condition. A new phase, $BaAl_2Si_2O_8$, forms in air after 500 h of thermal treatment at 800 °C, which is a direct consequence of continuous devitrification of the G18 glass. After 500 h of thermal treatment in the H_2/H_2O atmosphere, the peak intensities for the $BaCrO_4$ phase stay almost unchanged. This means the reaction between the AISI441 alloy and the G18 glass is not significantly affected by the atmosphere. The peaks of the Al_2SiO_4 phase are not as strong as those in the air condition, indicating that the reducing atmosphere suppresses the devitrification process. The peaks for the $BaFeSi_4O_{10}$ phase are almost the same as those in the air condition, again meaning that the interfacial reactions are not affected significantly by the atmospheres for the AISI441/G18 interface. $BaAl_2Si_2O_8$ is a stable phase, which also appears in the H_2/H_2O thermal treatment condition due to the devitrification of the G18 glass.

The XRD patterns of the AISI441/SABS-0 samples are shown in Fig. 11. The SABS-0 glass is relatively stable and only a few peaks are observed at different thermal treatment conditions. For the as-

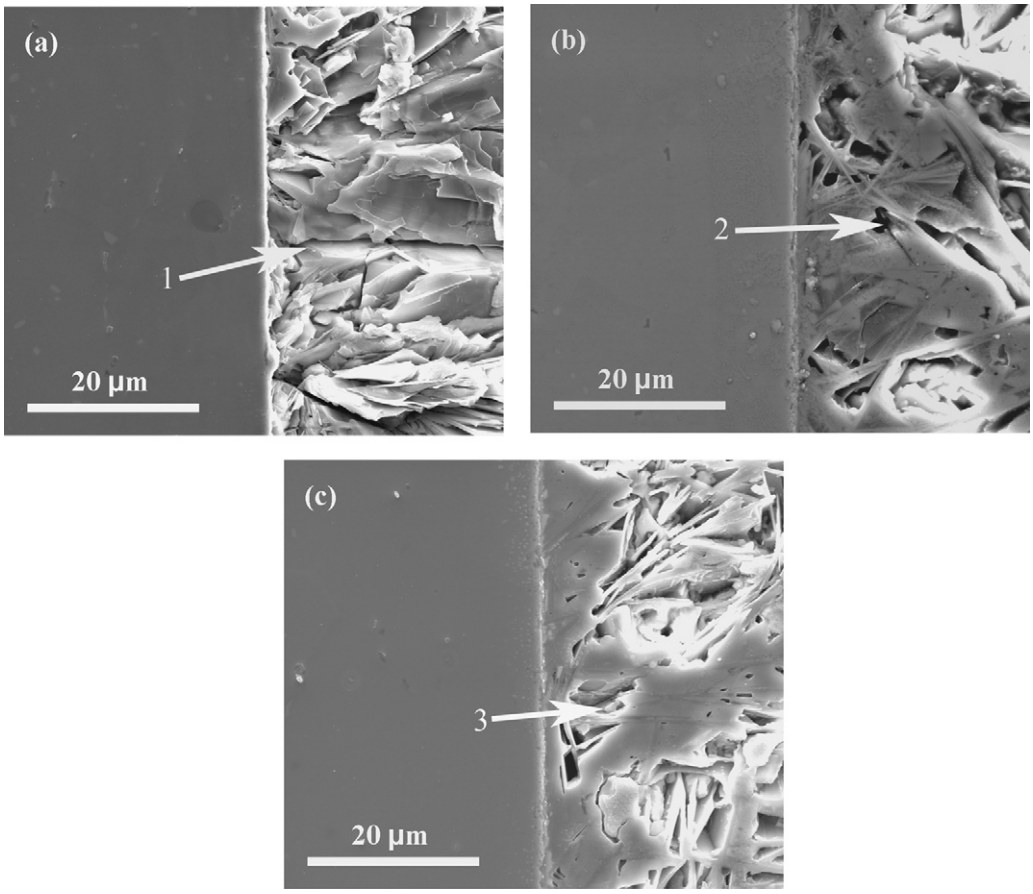

Fig. 6. Cross-section SEM images of the AISI441/G18 glass couple interface after thermal treatment at 800 °C in the H_2/H_2O atmosphere: (a) 100 h, (b) 200 h, and (c) 500 h. In each image, the left side is the AISI441 alloy and the right side is the G18 glass.

bonded sample, the crystalline phase is identified as La_2CrO_6. In the air condition, CrO_3 is the dominant Cr-containing vapor phase [33]. La_2O_3-containing glass system tends to form small, isolated, and phase-ordered clusters which are energetically favorable. These clusters generally contain La–O–La structural units [27]. These isolated La–O–La clusters act as nucleation sites for the devitrification of the SABS-0 glass [34,35]:

$$La_2O_3 + CrO_3 = La_2CrO_6 \quad (1)$$

After the thermal treatment, the XRD peaks for the La_2CrO_6 phase disappear and a new phase, $Sr_7Al_{12}O_{25}$, forms, along with a few very minor peaks. The $Sr_7Al_{12}O_{25}$ phase XRD peak intensities significantly increase for both the air and the H_2/H_2O atmosphere conditions. For both cases, the La_2CrO_6 phase cannot be detected anymore. $Sr_7Al_{12}O_{25}$ is the only crystalline phase identified at the interface. This means that La_2CrO_6 formation is limited to the bonding process. It is likely that the higher bonding temperature accelerates the vaporization and diffusion of the CrO_3 species. The La_2CrO_6 phase formation is mainly an interfacial event. The long-term thermal treatment at 800 °C probably leads to the disappearance of the La_2CrO_6 phase by decomposition and vaporization as well as the formation of $Sr_7Al_{12}O_{25}$ from the devitrification of the SABS-0 glass itself. The interaction between the AISI441 alloy and the SABS-0 glass is undetectable. The XRD pattern for the H_2/H_2O atmosphere condition is smoother with fewer peaks. The reducing atmosphere reduces the devitrification tendency of the SABS-0 glass.

The XRD patterns of the AISI441/SCAN2 samples are shown in Fig. 12. Sodium contributes to the lower glass softening temperature and higher coefficient of thermal expansion of the SCAN2 glass [30]. However, devitrification easily occurs at the AISI441/SCAN2 bonding temperature. The major crystalline phases after the bonding process can be identified as $NaAlSiO_4$ (hexagonal and cubic). The minor crystalline phases are $CaSiO_3$, $Ca_3Fe_2(SiO_4)_3$, and $CaFe_2O_4$. $NaAlSiO_4$ and $CaSiO_3$ form because of the devitrification of the SCAN2 glass itself. $Ca_3Fe_2(SiO_4)_3$ and $CaFe_2O_4$ form because of the Fe diffusion into and reaction with the SCAN2 glass. It is interesting to note that Cr species reaction with the SCAN2 glass is insignificant. After the bonding, $NaAlSiO_4$ forms quickly; both hexagonal and cubic phases are observed. The peaks of hexagonal $NaAlSiO_4$ are stronger. $CaSiO_3$ is also observed but the amount is low. $Ca_3Fe_2(SiO_4)_3$ and $CaFe_2O_4$ form in low amounts at the as-bonded condition. After the thermal treatment in air for 500 h, the amount of $NaAlSiO_4$ phase increases. The cubic phase amount increases more significantly. The amount of $CaSiO_3$ also increases after 500 h of thermal treatment in air even though the devitrification rate is slower. In contrast, the $Ca_3Fe_2(SiO_4)_3$ and $CaFe_2O_4$ phases do not increase much with the thermal treatment time. For the thermal treatment in the H_2/H_2O atmosphere for 500 h, the ratio of hexagonal to cubic $NaAlSiO_4$ stays similar to that of the as-bonded condition, which means the cubic $NaAlSiO_4$ phase is not as favorable in the H_2/H_2O atmosphere. The peak heights of the $CaSiO_3$, $Ca_3Fe_2(SiO_4)_3$, and $CaFe_2O_4$ phases increase compared to those of the $NaAlSiO_4$ phases. This is due to the relative content change for the devitrified phases and the reaction phases. The formation of the $NaAlSiO_4$ phases is less than that of the other phases in the H_2/H_2O atmosphere. So, the peak heights of the other phases increase more than those of the $NaAlSiO_4$ phases.

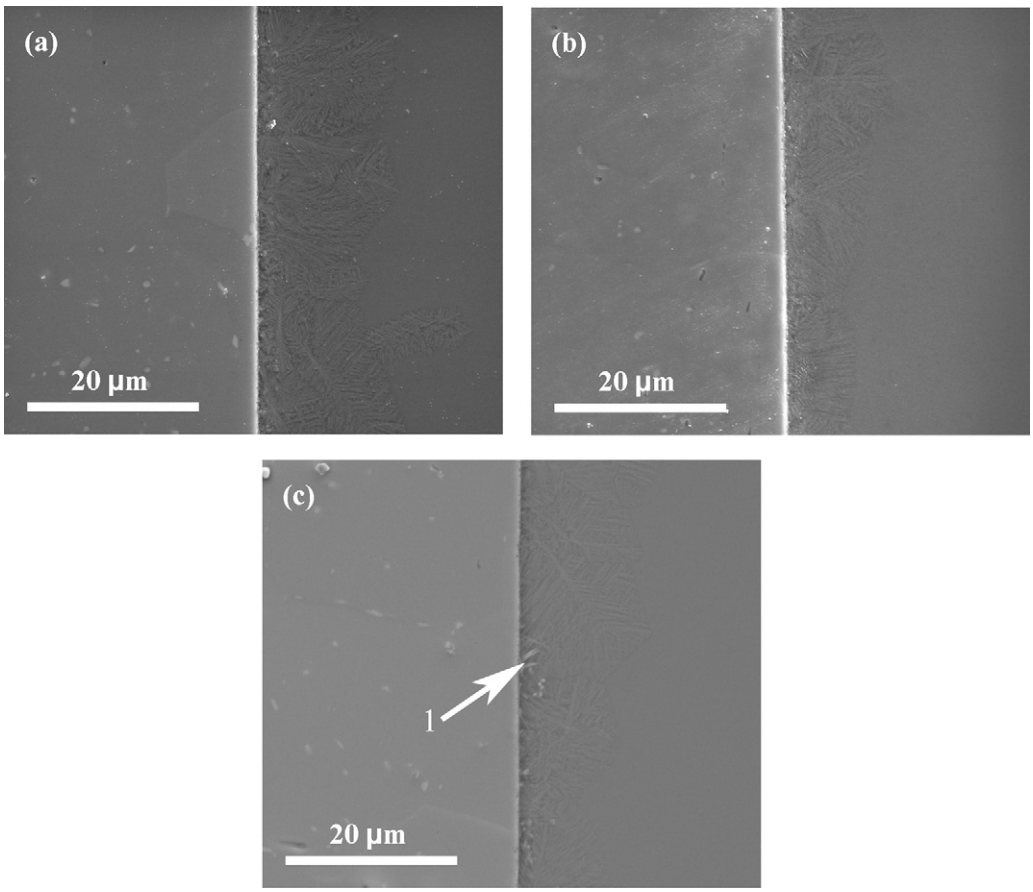

Fig. 7. Cross-section SEM images of the AISI441/SABS-0 glass couple interface after thermal treatment at 800 °C in the H_2/H_2O atmosphere: (a) 100 h, (b) 200 h, and (c) 500 h. In each image, the left side is the AISI441 alloy and the right side is the SABS-0 glass.

3.3. Devitrification, diffusion, and reaction at the interface

From the microstructure and the XRD results, it can be determined that at least three events: diffusion, chemical reaction, and devitrification of the glasses, occur during the thermal treatment of the AISI441/glass samples. This multi-event process at the interface can be illustrated as shown in Fig. 13.

For the AISI441/YSO-4 couple, the YSO-4 glass devitrification is the dominant event. Cr species diffuses into the YSO-4 glass. The chemical reaction at the interface is controlled by the diffusion process since diffusion must occur prior to the chemical reaction. After the chemical reaction, the metal/glass interface bonds. The diffusion of the AISI441 elements into the YSO-4 glass breaks the glass network structure and results in the further devitrification of the YSO-4 glass. The thick interfacial reaction layer of the AISI441/YSO-4 couple compromises the compatibility at the interface. For the AISI441/G18 couple, the devitrification process is dominant whereas the interfacial reaction is not severe. The G18 glass bonds with the AISI441 alloy due to the diffusion of Cr and Fe from the metal side. $BaCrO_4$ and $BaFeSi_4O_{10}$ are the reaction products at the interface, as shown in Fig. 10. The interface maintains its stability over the thermal treatment process. The morphology on the glass side changes due to the glass devitrification during the thermal treatment in both the air and the H_2/H_2O atmospheres. The layered crystalline phase leads to cracks and pores, which compromise the tightness of the sealing. For the AISI441/SABS-0 couple, La_2CrO_6 forms at the interface and devitrification occurs on the glass side close to the interface during the bonding process. This limited interaction provides chemical bonding between the AISI441 alloy and the SABS-0 glass. But there is no more interfacial reaction with the thermal treatment in either air or the H_2/H_2O atmosphere. The SABS-0 glass can maintain a stable interface with the AISI441 alloy and resist the effect of the Cr species vapor phase. Furthermore, the devitrification close to the interface initiated by the diffusion from the metal side stays within a limited range (Fig. 11) and no degradation is identified (Figs. 3 and 7). For the AISI441/SCAN2 couple, the interfacial reaction is extensive and led by the Fe diffusion from the metal side. Since the network connectivity of the SCAN2 glass is reduced by the glass modifier Na^+, the loose glass structure makes Fe diffusion into the glass much easier. The formation of $Ca_3Fe_2(SiO_4)_3$ and $CaFe_2O_4$ is more kinetically favorable than the reaction related to the Cr species because of the high Fe concentration at the interface. At the same time, the devitrified phases form during the bonding process and increase during the thermal treatment. The severe interfacial reaction indicates that the SCAN2 glass is a poor sealing glass and can easily separate from the AISI441 alloy.

The diffusion process mostly serves as the initiation point of the interfacial interaction and is complicated by the presence of multiple components in each glass and the AISI441 alloy, the chemical reaction, and the devitrification of the glass itself. If the diffusion of the Cr-containing species can be eliminated, the chemical reaction and the breakdown of the YSO-4 and the G18 glass network may be avoided. If the interfacial diffusion of Fe can be inhibited, the reaction and bonding failure between the AISI441 alloy and the SCAN2 glass may be avoided. The fundamental cause of the interfacial degradation can be attributed to the chromium and iron diffusion-induced chemical reaction and devitrification. Previous understanding regarding the interconnect/seal glass interaction [9,13,25,26,30] is mainly based on SEM microstructure and energy-

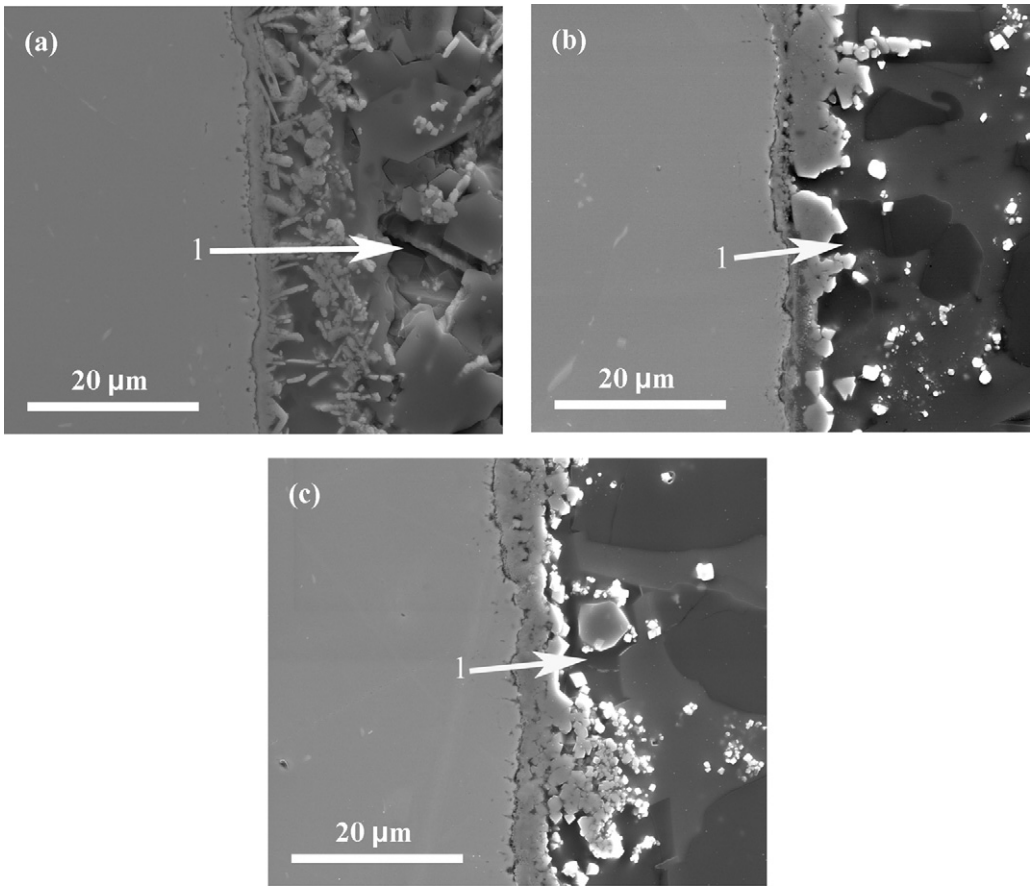

Fig. 8. Cross-section SEM images of the AISI441/SCAN2 glass couple interface before and after thermal treatment at 800 °C in H_2/H_2O atmosphere: (a) 100 h, (b) 200 h, and (c) 500 h. In each image, the left side is the AISI441 alloy and the right side is the SCAN2 glass.

dispersive X-ray spectroscopy (EDS) spot analysis. EDS, however, cannot detect specific compounds or crystalline phases. Reaction products, such as Cr_2O_3, $BaCrO_4$, and $SrCrO_4$, have been claimed only by comparing the EDS spot analysis results. Mn–Cr spinel layer is assumed to have formed at the Crofer 22 APU/glass interface and act as the active barrier layer for the diffusion of both the glass elements and the metal elements [36]. However, Cr_2O_3 and Mn–Cr spinel are not observed in the XRD patterns in the present study of the AISI441 alloy/glass couples, either because they are not present or the amount is too low. Little XRD work has been conducted to identify the reaction products or the crystalline phases in most of the interconnect/seal interfaces. This study provides insight into

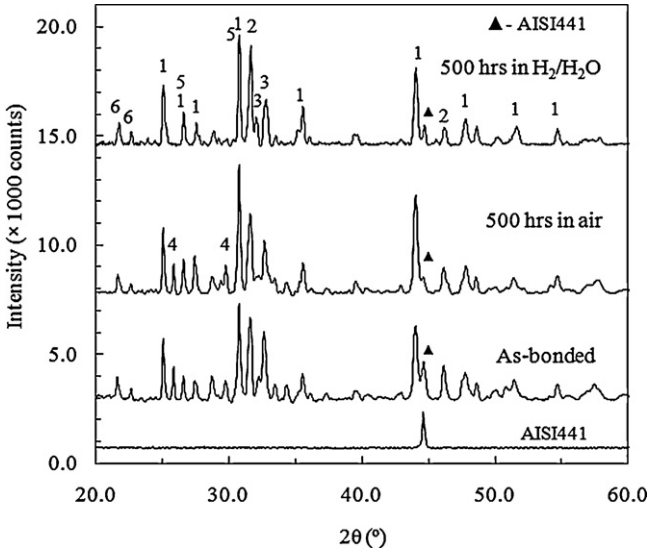

Fig. 9. XRD patterns at the AISI441/YSO-4 glass interface. (1) $SrSiO_3$; (2) Ca_3SiO_5; (3) Ca_2SiO_4; (4) $SrCrO_4$; (5) Sr_2CrO_4; and (6) Y_2SiO_5.

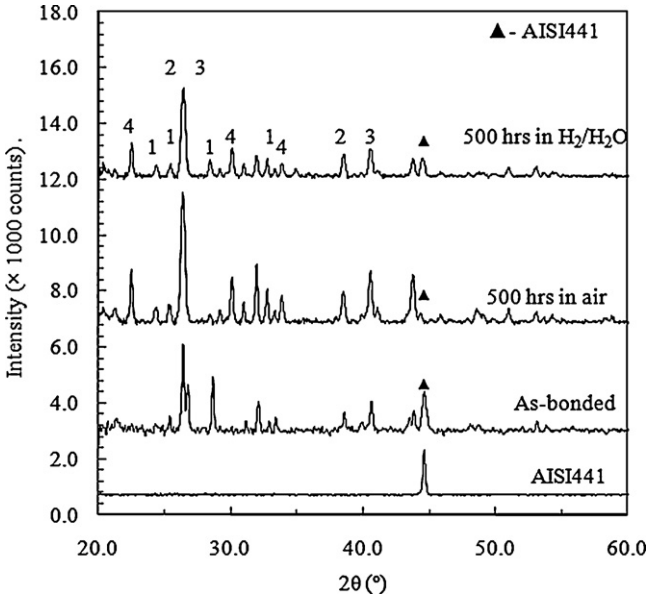

Fig. 10. XRD patterns at the AISI441/G18 glass interface. (1) $BaCrO_4$; (2) $BaFeSi_4O_{10}$; (3) Al_2SiO_4; and (4) $BaAl_2Si_2O_8$.

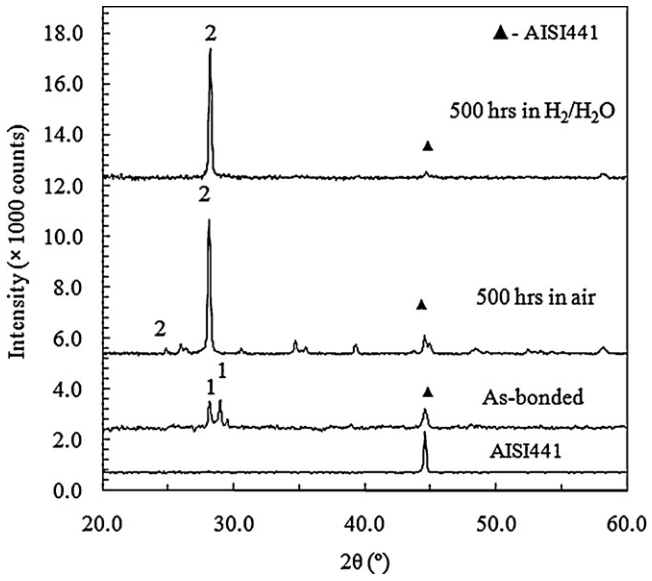

Fig. 11. XRD patterns at the AISI441/SABS-0 glass interface. (1) La_2CrO_6 and (2) $Sr_7Al_{12}O_{25}$.

the diffusion, chemical reaction, and glass devitrification phenomena at the interconnect/seal glass interface.

For the AISI441/SABS-0 couple, the interfacial interactions may have reached equilibrium after a certain thermal treatment time. Further reaction between the AISI441 alloy and the seal glass will not occur once the interface becomes chemically stable [37]. Pore- and crack-free interface and the identical crystalline phases at different thermal treatment time suggest that the SABS-0 glass is compatible with the AISI441 interconnect alloy. Generally, a few hundred micron thick glass seal is applied in planar solid oxide cells. The negligible interfacial layer and ~20 μm thick devitrified layer thickness at the AISI441/SABS-0 interface should not be a problem. The SABS-0 glass is a promising seal based on the results reported in this study.

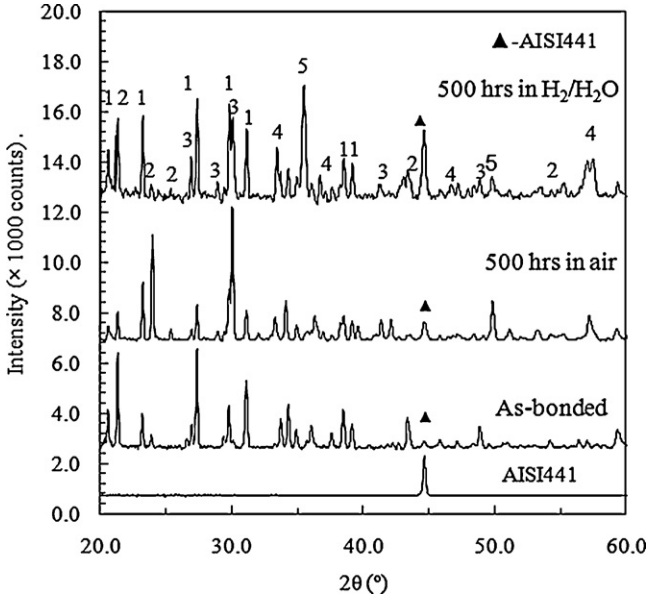

Fig. 12. XRD patterns at the AISI441/SCAN2 glass interface. (1) $NaAlSiO_4$ (hexagonal); (2) $NaAlSiO_4$ (cubic); (3) $CaSiO_3$; (4) $Ca_3Fe_2(SiO_4)_3$; and (5) $CaFe_2O_4$.

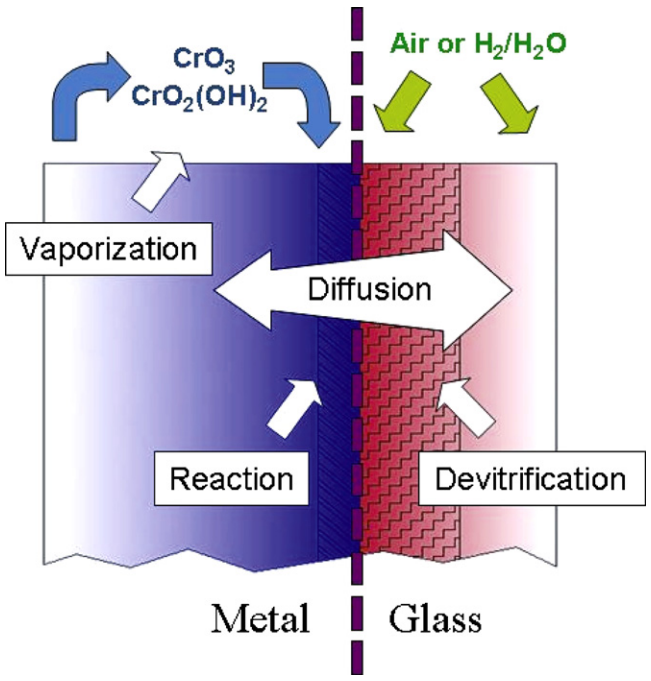

Fig. 13. Schematic view of the processes at the metal/glass interface during thermal treatment.

4. Conclusions

Interfacial compatibilities of AISI441/seal glass samples are investigated in air and H_2/H_2O atmospheres at 800 °C for up to 500 h. Glass composition strongly affects the interfacial behaviors. The YSO-4 and SCAN2 glasses react with the AISI441 alloy, forming an interfacial layer, pores, and cracks. The G18 glass devitrifies into a layered structure during the thermal treatment. The SABS-0 glass shows good bonding with the AISI441 alloy and has very limited devitrification. The H_2/H_2O atmosphere suppresses sealing glass devitrification and interfacial reaction. XRD analysis shows the devitrification phases vary with the sealing glass. Simultaneous diffusion, devitrification, and reaction occur at the interface and should be addressed separately. The study demonstrates that the SABS-0 glass is the most preferred sealing glass among the four glasses studied because of its interfacial stability and devitrification resistance.

Acknowledgments

This material is based on work supported by Department of Energy under Award Number DE-FC07-06ID14739. The SEM analysis was done in Nanoscale Characterization and Fabrication Laboratory, Virginia Tech. We thank ATI Allegheny Ludlum, Brackenrigde, PA for providing the AISI441 alloy sample.

References

[1] S. Elangovan, J.J. Hartvigsen, L.J. Frost, Int. J. Appl. Ceram. Technol. 4 (2007) 109–118.
[2] S.D. Park, J.M. Vohs, R.J. Gorte, Nature 404 (2000) 265–267.
[3] W. Schafer, A. Koch, U. HeroldSchmidt, D. Stolten, Solid State Ionics 86–88 (1996) 1235–1239.
[4] J. Akikusa, K. Adachi, K. Hoshino, T. Ishihara, Y. Takita, J. Electrochem. Soc. 148 (2001) A1275–A1278.
[5] P. Singh, N.Q. Minh, Int. J. Appl. Ceram. Technol. 1 (2004) 5–15.
[6] J.W. Fergus, Int. J. Hydrogen Energy 32 (2007) 3664–3671.
[7] P. Batfalsky, V.A.C. Haanappel, J. Malzbender, N.H. Menzler, V. Shemet, I.C. Vinke, R.W. Steinbrech, J. Power Sources 155 (2006) 128–137.
[8] J.W. Fergus, Mater. Sci. Eng. A 397 (2005) 271–283.

[9] Z.G. Yang, K.D. Meinhardt, J.W. Stevenson, J. Electrochem. Soc. 150 (2003) A1095–A1101.
[10] C.L. Chu, J. Lee, S.Y. Lee, J. Ceram. Process. Res. 9 (2008) 338–342.
[11] B.C.H. Steele, A. Heinzel, Nature 414 (2001) 345–352.
[12] S. Chandra-Ambhorn, Y. Wouters, L. Antoni, F. Toscan, A. Galerie, J. Power Sources 171 (2007) 688–695.
[13] N.H. Menzler, D. Sebold, M. Zahid, S.M. Gross, T. Koppitz, J. Power Sources 152 (2005) 156–167.
[14] M.J. Pascual, A. Guillet, A. Duran, J. Power Sources 169 (2007) 40–46.
[15] M. Stanislowski, J. Froitzheim, L. Niewolak, W.J. Quadakkers, K. Hilpert, T. Markus, L. Singheiser, J. Power Sources 164 (2007) 578–589.
[16] S.P. Simner, M.D. Anderson, G.G. Xia, Z. Yang, L.R. Pederson, J.W. Stevenson, J. Electrochem. Soc. 152 (2005) A740–A745.
[17] Z.G. Yang, G.G. Xia, C.M. Wang, Z.M. Nie, J. Templeton, J.W. Stevenson, P. Singh, J. Power Sources 183 (2008) 660–667.
[18] D. Bahadur, N. Lahl, K. Singh, L. Singheiser, K. Hilpert, J. Electrochem. Soc. 151 (2004) A558–A562.
[19] M. Bram, S. Reckers, P. Drinovac, J. Monch, R.W. Steinbrech, H.P. Buchkremer, D. Stover, J. Power Sources 138 (2004) 111–119.
[20] R. Zheng, S.R. Wang, H.W. Nie, T.L. Wen, J. Power Sources 128 (2004) 165–172.
[21] N.P. Bansal, E.A. Gamble, J. Power Sources 147 (2005) 107–115.
[22] J.W. Fergus, J. Power Sources 147 (2005) 46–57.
[23] A. Flugel, M.D. Dolan, A.K. Varshneya, Y. Zheng, N. Coleman, M. Hall, D. Earl, S.T. Misture, J. Electrochem. Soc. 154 (2007) B601–B608.
[24] C. Story, K. Lu, W.T. Reynolds, D. Brown, Int. J. Hydrogen Energy 33 (2008) 3970–3975.
[25] Y.S. Chou, J.W. Stevenson, P. Singh, J. Electrochem. Soc. 154 (2007) B644–B651.
[26] K.D. Meinhardt, D.S. Kim, Y.S. Chou, K.S. Weil, J. Power Sources 182 (2008) 188–196.
[27] M.K. Mahapatra, K. Lu, R.J. Bodnar, Appl. Phys. A 95 (2009) 493–500.
[28] T. Jin, K. Lu, J. Power Sources 195 (2010) 195–203.
[29] M.K. Mahapatra, K. Lu, J. Mater. Sci. 44 (2009) 5569–5578.
[30] F. Smeacetto, M. Salvo, A. Ferraris, V. Casalegno, P. Asinari, J. Eur. Ceram. Soc. 28 (2008) 611–616.
[31] B.D. Cullity, Elements of X-ray Diffraction, second ed., Addision–Wesley Publishing Company Inc., Philippines, 1978.
[32] P.D. Jablonski, D.E. Alman, J. Power Sources 180 (2008) 433–439.
[33] D. Caplan, M. Cohen, J. Electrochem. Soc. 108 (1961) 438–442.
[34] T. Schaller, J.F. Stebbins, M.C. Wilding, J. Non-Cryst. Solids 243 (1999) 146–157.
[35] M.C. Wilding, A. Navrotsky, J. Non-Cryst. Solids 265 (2000) 238–251.
[36] Y.S. Chou, J.W. Stevenson, P. Singh, J. Power Sources 185 (2008) 1001–1008.
[37] J.A. Pask, Chemical bonding at glass-to-metal interfaces, in: W.E. Moddeman, C.W. Merten, D.P. Kramer (Eds.), Technology of Glass, Ceramic, or Glass-Ceramic to Metal Sealing, The American Society of Mechanical Engineers, New York, 1987, pp. 1–7.